JGR Atmospheres

RESEARCH ARTICLE
10.1029/2023JD040294

Unraveling the Role of the Interdecadal Pacific Oscillation in Recent Tropical Expansion via Large-Ensemble Simulations

Mingna Wu[1,2], Tianjun Zhou[3,4], Chao Li[5], Bo Wu[3], and Jie Jiang[3]

[1]Department of Atmospheric Science, School of Environmental Studies, China University of Geosciences, Wuhan, China, [2]Key Laboratory of Meteorological Disaster (KLME), Ministry of Education & Collaborative Innovation Center on Forecast and Evaluation of Meteorological Disasters (CIC-FEMD), Nanjing University of Information Science & Technology, Nanjing, China, [3]State Key Laboratory of Numerical Modeling for Atmospheric Sciences and Geophysical Fluid Dynamics (LASG), Institute of Atmospheric Physics, Chinese Academy of Sciences, Beijing, China, [4]University of Chinese Academy of Sciences, Beijing, China, [5]Max Planck Institute for Meteorology, Hamburg, Germany

Abstract Observational evidence has shown that the Earth's tropics have widened since 1980. However, climate models underestimate the observed tropical expansion rate, with a large spread among individual models. The proposal of internal variability to account for model–observation differences is hindered by the limited availability of sufficient realizations from models in the Coupled Model Intercomparison Project (CMIP), restricting the accuracy of quantitative contribution estimation. The emergence of a single model initial-condition large ensemble provides a new opportunity to quantify the role of internal variability. Here, using large-ensemble simulations from two individual models complemented with CMIP Phase 6 (CMIP6) simulations, we show evidence that the recent widening of the tropics is mainly caused by internal variability related to the Interdecadal Pacific Oscillation (IPO). The positive-to-negative phase transition of the IPO from 1980 to 2014 reduced the meridional tropospheric temperature gradient, resulting in poleward shifts in tropical edges. After adjusting the IPO trends simulated by individual realizations to ensure consistency with the observations, the IPO phase transition can account for at least 73% (66%) of the observed tropical expansion rate in the Northern Hemisphere based on the metric of the meridional stream function (surface zonal wind). The IPO is also essential for shaping tropical expansion-related precipitation changes. Our results underscore the significance of considering internal variability when explaining model–observation differences and understanding intermodel uncertainty.

Plain Language Summary The edge of the tropics has shifted poleward over the past few decades, a phenomenon referred to as tropical expansion. However, existing climate models exhibit underestimate of the observed tropical expansion rate and show a large spread in the simulated rates. Although internal climate variability is suggested as an explanation for the difference between observations and climate models and the spread across models, it is difficult to quantitatively estimate its contribution due to the insufficient use of climate models. With the utilization of two large-ensemble simulations with an ample number of independent realizations, our findings reveal that the internal variability associated with the Interdecadal Pacific Oscillation (IPO) plays a significant role in contributing to both model–observation differences and intermodel spread in the tropical expansion rate. Expanding on the benefits of large ensembles, we quantify the relative contribution of the IPO, suggest likely physical mechanisms, and investigate the impact of the IPO on tropical expansion-related precipitation changes. Our work provides a useful reference for how large-ensemble simulations help explain model–observation inconsistencies and reveals the essential role of IPO-related internal variability in the prediction of tropical expansion rates.

Key Points:

- The Interdecadal Pacific Oscillation (IPO) explains 66%–73% of the observed tropical expansion rate in the Northern Hemisphere from 1980 to 2014
- The recent shift in the IPO phase modulates the width of the tropics by reducing the meridional tropospheric temperature gradient
- The IPO is essential for shaping tropical expansion-related precipitation changes

Correspondence to:
T. Zhou,
zhoutj@lasg.iap.ac.cn

Citation:
Wu, M., Zhou, T., Li, C., Wu, B., & Jiang, J. (2024). Unraveling the role of the Interdecadal Pacific Oscillation in recent tropical expansion via large-ensemble simulations. *Journal of Geophysical Research: Atmospheres*, *129*, e2023JD040294. https://doi.org/10.1029/2023JD040294

Received 25 OCT 2023
Accepted 11 MAY 2024

Author Contributions:
Conceptualization: Mingna Wu, Tianjun Zhou, Chao Li
Formal analysis: Mingna Wu
Writing – original draft: Mingna Wu
Writing – review & editing: Mingna Wu, Tianjun Zhou, Chao Li, Bo Wu, Jie Jiang

1. Introduction

The edges of the tropics have shifted poleward over the past few decades, which is referred to as tropical expansion (Fu et al., 2006; Hu & Fu, 2007; Hudson et al., 2006; Seidel & Randel, 2007; Seidel et al., 2008). Tropical expansion influences hydrological cycles within both the tropics and extratropics, resulting in shifts in dry regions and rain belts (Brönnimann et al., 2015; Feng & Fu, 2013; Post et al., 2014; Scheff & Frierson, 2012; Schmidt & Grise, 2017), adjustments in ocean upwelling processes and marine bioproductivity (Irwin & Oliver, 2009; Moore et al., 2018; Polovina et al., 2008; Rykaczewski et al., 2015), and modifications of tropical cyclone trajectories (Sharmila & Walsh, 2018; Studholme & Gulev, 2018). The observed magnitude of recent

tropical expansion is approximately 0.25°–0.5° latitude per decade (Allen & Kovilakam, 2017; N. A. Davis & Birner, 2017; Grise & Davis, 2020; Grise et al., 2018; Staten et al., 2020, 2018; Studholme & Gulev, 2018). However, state-of-the-art climate models underestimate the tropical expansion rate relative to observations (Hu et al., 2013; Johanson & Fu, 2009; Quan et al., 2014; Seidel et al., 2008) and exhibit high uncertainty in the tropical expansion rate (Grise & Davis, 2020). The difference among climate models in replicating observed historical changes may hinder the reliability of both near-term predictions and long-term projections. Hence, gaining a deeper understanding of model–observation differences is important for the climate community.

Previous studies have suggested that tropical expansion may have resulted from internal climate variability, particularly connected to sea surface temperature (SST) variations in the Pacific Ocean (Allen & Kovilakam, 2017; Chen et al., 2008; Grise et al., 2019; Lu et al., 2008; Mantsis et al., 2017; Simpson, 2018). For example, SST variations related to the El Niño-Southern Oscillation (ENSO) or Pacific Decadal Oscillation/Interdecadal Pacific Oscillation (PDO/IPO), which are the main internal modes in the Pacific characterized by interannual to interdecadal SST fluctuations as results of air-sea interaction (Henley et al., 2015; Mantua & Hare, 2002), can modulate the meridional temperature gradient and hence the tropical width (Seo et al., 2023; Yang et al., 2023). Since internal variability can result in distinct states between the observed and simulated fluctuations (Notz, 2015), both model–observation differences and intermodel spread in the tropical expansion rate may originate from internal variability. Although the influence of internal variabilities, such as the ENSO, PDO and IPO, has been recorded in previous studies, less effort has been devoted to determining their quantitative contributions and the mechanisms through which they influence the extent of the tropical belt. Furthermore, there is a need to clarify the extent to which the internal decadal variability can modulate changes in precipitation associated with poleward migration of the tropical boundary.

Employing models with a larger number of ensemble members, as opposed to relying on a single realization, is crucial for understanding the function of internal variability. While previous studies based on the analysis of CMIP models have enhanced our understanding of internal variability (Allen et al., 2012; N. A. Davis & Birner, 2017; Grise & Davis, 2020; Grise et al., 2019; Tao et al., 2015), it is challenging to entirely disentangle the influence of external forcings from the internal variability with a limited number of realizations (Deser et al., 2020). Compared with CMIP models, a single model initial-condition large ensemble with sufficient independent realizations is an effective tool for estimating the relative contribution of internal variability (Deser et al., 2020; Yeh et al., 2021). This occurs because, in initial-condition large-ensemble simulations, all the members share the same external forcing but are initiated with differing initial states (Maher et al., 2019). Hence, in contrast to the CMIP ensemble, the differences among the realizations in large-ensemble simulations can be attributed solely to internal climate variability.

Here, we revisit recent tropical expansion with an emphasis on internal variability. With the use of initial-condition large-ensemble simulations involving two models, namely, the Max Planck Institute for Meteorology (MPI-M) climate model with 100 realizations (hereafter referred to as MPI-GE) and the CESM1 model with 40 realizations (hereafter referred to as CESM-LE), our goal is to address the following questions: (a) which internal variability mode can account for both model–observation differences and the intermodel spread in the recent tropical expansion rate? (b) To what extent and through which process can this internal variability modulate changes in the tropical belt width? (c) What role does this internal variability play in shaping precipitation changes associated with tropical expansion?

2. Data and Methods

2.1. Observations and Reanalysis

Previous studies have suggested that modern reanalysis data are more accurate in reflecting past changes in the tropical width because early generation reanalysis data exhibit significant deviations from mass conservation throughout the historical period (N. A. Davis & Davis, 2018). We use the monthly mean meridional winds from four modern reanalysis data sets to calculate the poleward edge of the tropical belt: (a) the ECMWF Interim Reanalysis (ERAIM) data set (Dee et al., 2011); (b) the European Centre for Medium-Range Weather Forecasts (ECMWF) Reanalysis 5th Generation (ERA5) data set (Hersbach et al., 2020); (c) the Modern Era Retrospective Analysis for Research and Applications 2 (MERRA2) data set (Gelaro et al., 2017); and (d) the Japanese Meteorological Agency 55-year Reanalysis (JRA55) data set (Kobayashi et al., 2015). The monthly mean SST is obtained from the Extended Reconstructed Sea Surface Temperature version 5 (ERSST v5) data set (B. Huang

et al., 2017). The precipitation data are derived from the Global Precipitation Climatology Project (GPCP) monthly product version 2.3 (Adler et al., 2003).

2.2. Climate Simulations

For model–observation comparisons, we mainly use large-ensemble simulations from MPI-GE (Maher et al., 2019), which contains 100 members. All MPI-GE members are obtained by the same model (MPI-ESM1.1) and share identical time-varying external forcings. Additional details regarding the design of the MPI-GE can be found in Maher et al. (2019). To maintain consistency with the observations, the overall period (1980–2014) in MPI-GE combines the 1980–2005 period of historical simulations with the 2006–2014 period of RCP8.5 simulations. We further employ CESM-LE with 40 ensemble members (Kay et al., 2015) to verify the results obtained from MPI-GE.

To complement the data derived from large ensembles, we also use the historical simulations (1980–2014) of 35 models from the CMIP6 (Eyring et al., 2016) (refer to Table 1 for more information). We employ the first ensemble member (r1i1p1f1) to assign an equal weight to each model, except for two cases in which the weight cannot be assigned (i.e., r1i1p1f2 is used for HadGEM3-GC31-LL, and r1i1p1f3 is adopted for CNRM-CM6-1, CNRM-ESM2-1, MIROC-ES2L, and UKESM1-0-LL). A common period (1980–2014) in both the observations and models is selected to calculate the tropical expansion trend.

2.3. Defining the Edge of the Tropical Belt

Various metrics, which can be categorized as dynamic, hydrological, thermal or chemical indicators, have been utilized to measure the edge of tropical belts (Staten et al., 2018; Xian et al., 2021). Among these metrics, the meridional overturning stream function is mostly used to describe the width of the tropics (Cook, 2003). Hence, the poleward edge of the tropical belt can be computed by the zero-crossing latitude of the meridional overturning stream function at 500 hPa over the subtropics (PSI500) (Allen et al., 2012; S. M. Davis & Rosenlof, 2012; Grise & Davis, 2020; Hu & Fu, 2007; Nguyen et al., 2013). To reduce the uncertainty in the different metrics, we also use the surface zonal wind to estimate the edge of the tropics, which refers to the latitudinal direction in the subtropics where the zonal-mean zonal wind at 1000 hPa (USFC) changes (N. A. Davis & Birner, 2017). In this study, we adopt the Tropical-width Diagnostics code package (TropD) to calculate the PSI500 and USFC metrics (Adam et al., 2018).

2.4. Statistical Analysis

This study mainly focused on the annual mean variations in the tropical width. We first applied a 7-year running mean to the annual mean fields to extract interdecadal signals. Based on MPI-GE simulations, the impacts of external forcings and internal variability on changes in the tropical width can be captured using the mean of all ensemble members and the deviations in the individual members from the ensemble mean, respectively (Maher et al., 2019). The IPO index can be calculated as the contrast in regionally averaged internal SST anomalies between the equatorial Pacific region (10°S–10°N, 170°E−90°W) and the average of the northwestern (25°–45°N, 140°E−145°W) and southwestern (50°–15°S, 150°E−160°W) Pacific regions (Henley et al., 2015). The Niño 3.4 index can be computed by the average SST anomaly over the 5°N–5°S, 170–120°W region.

2.5. Method for Adjusting the Phase Transition of the IPO

Here we estimate the relative contribution of IPO to the recent tropical expansion by adjusting the IPO trends in each individual member of large-ensemble simulations based on the observed IPO change. For each member i, the tropical expansion rate ($\frac{\partial \mathrm{Trop}D(i,t)}{\partial t}$) during the 1980–2014 period can be expressed as:

$$\frac{\partial \mathrm{Trop}D(i,t)}{\partial t} = \frac{\partial \mathrm{Trop}D_{\mathrm{forced}}(t)}{\partial t} + \frac{\partial \mathrm{Trop}D_{\mathrm{internal}}(i,t)}{\partial t}, i = 1,2,3,\ldots,N \quad (1)$$

where $\frac{\partial \mathrm{Trop}D_{\mathrm{forced}}(i,t)}{\partial t}$ denotes the forced tropical edge shift, which is the same for each individual member in large ensembles, and $\frac{\partial \mathrm{Trop}D_{\mathrm{internal}}(i,t)}{\partial t}$ is the internally driven tropical edge shift.

Table 1
Information of the CMIP6 Climate Models Used in This Study

Model	Institution	Resolution (Lat × Lon)	Experiment
ACCESS-CM2	CSIRO/Australia	144 × 192	Historical
ACCESS-ESM1-5	CSIRO/Australia	145 × 192	Historical
AWI-CM-1-1-MR	AWI/Germany	192 × 384	Historical
BCC-CSM2-MR	BCC/China	160 × 320	Historical
CAMS-CSM1-0	CAMS/USA	160 × 320	Historical
CanESM5	CCCMA/Canada	64 × 128	Historical
CESM2-WACCM	NCAR/USA	192 × 288	Historical
CMCC-CM2-SR5	CMCC/Italy	192 × 288	Historical
CNRM-CM6-1	CNRM-CERFACS/France	128 × 256	Historical
CNRM-ESM2-1	CNRM-CERFACS/France	128 × 256	Historical
EC-Earth3	EC-Earth-Consortium/EU	256 × 512	Historical
EC-Earth3-Veg	EC-Earth-Consortium/EU	256 × 512	Historical
EC-Earth3-Veg-LR	EC-Earth-Consortium/EU	256 × 512	Historical
FGOALS-f3-L	CAS/China	180 × 360	Historical
FGOALS-g3	CAS/China	90 × 180	Historical
GFDL-CM4	NOAA- GFDL/USA	180 × 288	Historical
GFDL-ESM4	NOAA- GFDL/USA	180 × 288	Historical
GISS-E2-1-G	GISS-GISS/USA	90 × 144	Historical
HadGEM3-GC31-LL	MOHC/UK	144 × 192	Historical
IITM-ESM	CCCR-IITM/India	94 × 192	Historical
IPSL-CM6A-LR	IPSL/France	143 × 144	Historical
INM-CM4-8	INM/Russia	120 × 180	Historical
INM-CM5-0	INM/Russia	120 × 180	Historical
KACE-1-0-G	NIMS-KMA/South Korea	145 × 192	Historical
MCM-UA-1-0	UA/USA	80 × 96	Historical
MIROC6	MIROC/Japan	128 × 256	Historical
MIROC-ES2L	MIROC/Japan	64 × 128	Historical
MPI-ESM1-2-HR	MPI-M/Germany	192 × 384	Historical
MPI-ESM1-2-LR	MPI-M/Germany	96 × 192	Historical
MRI-ESM2-0	MRI/Japan	160 × 320	Historical
NESM3	NUIST/China	96 × 192	Historical
NorESM2-LM	NCC/Norway	96 × 144	Historical
NorESM2-MM	NCC/Norway	192 × 288	Historical
TaiESM1	AS-RCEC/Taiwan	192 × 288	Historical
UKESM1-0-LL	MOHC/UK	144 × 192	Historical

Based on Equation 1, the contribution of the IPO to the observed tropical expansion can be quantified by adjusting the IPO phase to be consistent with the observations to each individual member of large-ensemble simulations via the following two steps (X. Huang et al., 2020; Salzmann & Cherian, 2015; Wu et al., 2021).

First, we exclude the original IPO-related tropical expansion rates of each member ($r(i)_{\mathrm{Trop}D,\mathrm{IPO}} \cdot \frac{\partial \mathrm{IPO}(i,t)}{\partial t}$) from the large-ensemble simulations.

Second, we add the observed IPO-related tropical expansion rates back to each member through regression ($r(i)_{\mathrm{Trop}D,\mathrm{IPO}} \cdot \frac{\partial \mathrm{IPO}_{\mathrm{OBS}}(i,t)}{\partial t}$). Hence, Equation 1 becomes:

$$\frac{\partial \mathrm{Trop}D_{\mathrm{adj}}(i,t)}{\partial t} = \frac{\partial \mathrm{Trop}D_{\mathrm{forced}}(t)}{\partial t} + \frac{\partial \mathrm{Trop}D_{\mathrm{internal}}(i,t)}{\partial t} - r(i)_{\mathrm{Trop}D,\mathrm{IPO}} \cdot \frac{\partial \mathrm{IPO}(i,t)}{\partial t} + r(i)_{\mathrm{Trop}D,\mathrm{IPO}} \cdot \frac{\partial \mathrm{IPO}_{\mathrm{OBS}}(i,t)}{\partial t}, i = 1,2,3,\ldots,N \quad (2)$$

which can be simplified as:

$$\frac{\partial \mathrm{Trop}D_{\mathrm{adj}}(i,t)}{\partial t} = \frac{\partial \mathrm{Trop}D_{\mathrm{forced}}(t)}{\partial t} + \frac{\partial \mathrm{Trop}D_{\mathrm{internal}}(i,t)}{\partial t} + r(i)_{\mathrm{Trop}D,\mathrm{IPO}} \cdot \left(\frac{\partial \mathrm{IPO}_{\mathrm{OBS}}(i,t)}{\partial t} - \frac{\partial \mathrm{IPO}(i,t)}{\partial t}\right), i = 1,2,3,\ldots,N \quad (3)$$

The magnitude of the adjustment term depends on the difference in the IPO trend between the observations and simulations ($\frac{\partial \mathrm{IPO}_{\mathrm{OBS}}(i,t)}{\partial t} - \frac{\partial \mathrm{IPO}(i,t)}{\partial t}$). After adjustment, all the large ensemble members are influenced by the same observed IPO phase transition.

Finally, through the comparison of the tropical expansion rates before and after adjustment ($\frac{\partial \mathrm{Trop}D(i,t)}{\partial t}$ and $\frac{\partial \mathrm{Trop}D_{\mathrm{adj}}(i,t)}{\partial t}$), we can quantitatively estimate the contribution of the IPO phase transition to recent expansion rates.

2.6. Removing the Influence of ENSO From the Precipitation Field

On an interannual timescale, the tropical belt contracts during El Niño events and expands during La Niña events (Lu et al., 2008). To remove the effect of ENSO from the precipitation field, we subtract the ENSO-congruent component of precipitation from each grid as follows:

$$\mathrm{Pr}_{\mathrm{non-ENSO}} = \mathrm{Pr} - \mathrm{Pr}_{\mathrm{ENSO-related}} \quad (4)$$

where Pr, $\mathrm{Pr}_{\mathrm{non\text{-}ENSO}}$, and $\mathrm{Pr}_{\mathrm{ENSO\text{-}related}}$ are the original precipitation field, the precipitation field with the effect of the ENSO removed and the ENSO-related precipitation field, respectively.

The ENSO-related precipitation field ($\mathrm{Pr}_{\mathrm{ENSO-related}}$) can be obtained through linear regression (Schmidt & Grise, 2017):

$$\mathrm{Pr}_{\mathrm{ENSO-related}} = \mathrm{reg}(\mathrm{Pr},\mathrm{Niño\ 3.4}) \cdot \mathrm{Niño3.4} \quad (5)$$

where reg(Pr,Niño 3.4) is the slope of the linear regression between the precipitation field and the Niño 3.4 index.

2.7. Tropical Expansion-Related Precipitation Trend

We extracted the tropical expansion-related precipitation trend following Thompson et al. (2000), Zhou and Li (2008), and Schmidt and Grise (2017). First, we regressed the precipitation onto the monthly time series of the PSI500 index on the interannual timescale. To extract interannual signals, we removed the trend, seasonal cycle, and 7-year running average from the precipitation field. The trend and 7-year running average were also removed from the time series of the PSI500 index. Subsequently, we multiplied the resultant regression coefficients by the linear trend in the PSI500 index. Therefore, the portion of the precipitation trend linearly congruent with year-to-year changes in the tropical width could be obtained.

3. Results

3.1. Forced Response and Role of Internal Variability

We first examine the annual mean changes in two commonly used metrics of the tropical belt edge: PSI500 and USFC (Figure 1). The observations exhibit multidecadal variability throughout the 1980–2014 period in both hemispheres, with significant poleward shifts in the tropical belt edge (Figure 1). According to the observations, the average tropical expansion rates (and ranges) computed from the various reanalysis data in the Northern Hemisphere are 0.25 (−0.07–0.64)° (35 years)$^{-1}$ for the PSI500 metric (Figures 1a and 2a) and 0.46 (0.23–0.73)°

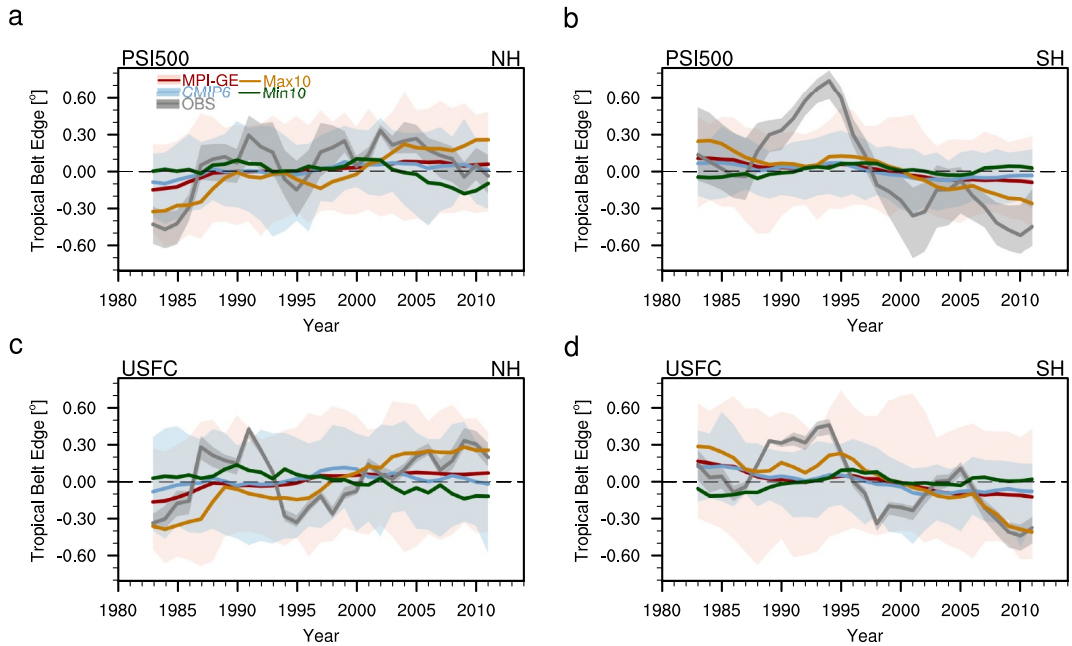

Figure 1. Changes in the tropical belt edge over the 1980–2014 period. Time series of the subtropical edge latitude anomaly (units: degree of latitude) of the tropical belt relative to the 1980–2014 means over the (a) Northern Hemisphere and (b) Southern Hemisphere based on the PSI500 metric. The gray line denotes the average of the four reanalysis data sets, with the shading indicating the spread. The red (blue) line is derived from the ensemble mean of 100 (35) MPI-GE members (CMIP6 models), while the shading with the corresponding color indicates the intermember (intermodel) spread of all ensemble members (models). The yellow (green) line denotes the mean of 10 ensemble members showing the highest (lowest) tropical expansion rate. (c, d) As in (a, b) but for the USFC metric.

(35 years)$^{-1}$ for the USFC metric (Figures 1c and 2c). Compared with the observations, the CMIP6 multimodel ensemble mean (MME) of each individual member exhibits a slight widening of the tropical belt (Figures 1a and 1c), with a trend of 0.12° (35 years)$^{-1}$ for the PSI500 metric (Figures 2a) and 0.11° (35 years)$^{-1}$ for the USFC metric (Figure 2c). In the observations, the tropical expansion rate in the Southern Hemisphere is −0.82 (−1.56 to −0.26)° (35 years)$^{-1}$ for the PSI500 metric (Figure 2b) and −0.60 (−0.85 to −0.39)° (35 years)$^{-1}$ for the USFC metric (Figure 2d). The contribution of external forcings measured by the CMIP6 multimodel ensemble mean is −0.17 (−0.24)° (35 years)$^{-1}$ based on the PSI500 (USFC) metric, which is approximately one-fifth (one half) that of the observed trend (Figures 2b and 2d).

Although the CMIP6 MME failed to reproduce the observed magnitude of the tropical expansion rates, the observations are within the 5th to 95th percentile span of the CMIP6 model realizations in both hemispheres (Figure 2). Moreover, the intermodel spread of the CMIP6, measured by the standard deviation of the tropical expansion rate, is 0.35° (35 years)$^{-1}$ for the Northern Hemisphere and 0.26° (35 years)$^{-1}$ for the Southern Hemisphere, which are greater than those of the CMIP6 MME. Note that the different reanalysis data exhibit uncertainty in terms of the tropical expansion rate based on the PSI500 metric (Figures 1a and 1b), which may be associated with their varying ability to preserve mass conservation (N. A. Davis & Davis, 2018).

For a more in-depth analysis of the impact of internal variability, we employed MPI-GE to investigate whether internal variability plays a role in recent tropical expansion. The ensemble mean of MPI-GE reasonably reproduces the climatological location of the tropical belt edge for both metrics (figure not shown), adding confidence to our analysis based on MPI-GE. The externally forced change in the tropical belt, represented by the average of all MPI-GE members, exhibits monotonic widening over time (Figure 1). The MPI-GE ensemble mean shows that the direction of the change in the tropical belt edge is consistent with the observations, suggesting the positive influence of external forcing. However, the substantial impact of internal variability results in notable uncertainty in MPI-GE (Figure 1). Similar to the CMIP6 models, the observed changes fall within the spread among the MPI-GE ensemble members (Figure 1), especially in the Northern Hemisphere (Figures 1a and 1c).

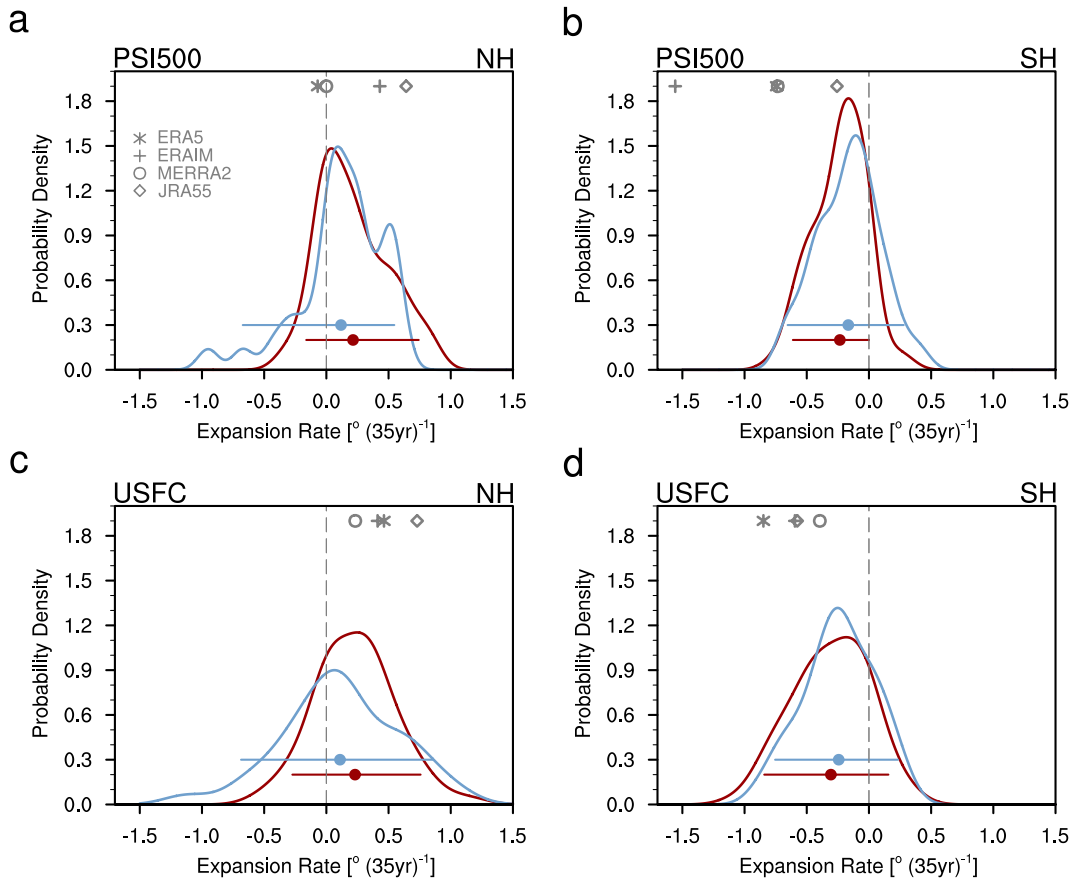

Figure 2. Probability density of the trends in the subtropical edge latitude of the tropical belt. MPI-GE members (red line) and CMIP6 models (blue line) for the (a) Northern Hemisphere and (b) Southern Hemisphere based on the PSI500 metric. The dots and vertical lines with the corresponding colors denote the ensemble mean and 5th to 95th percentile range, respectively. The asterisk, circle, square and diamond denote the trends derived from the ERA5, ERAIM, MERRA and JRA55 data, respectively. (c, d) As in (a, b) but for the USFC metric.

Furthermore, the intermember range of MPI-GE in both hemispheres encompasses the spread among the CMIP6 models, confirming the role of internal variability (Figure 1).

Quantitatively, the expansion rates of MPI-GE ranged from −0.35 (−0.80)° to 0.86 (0.32)° (35 years)$^{-1}$ in the Northern (Southern) Hemisphere, with an ensemble mean of 0.21 (−0.23)° (35 years)$^{-1}$ based on the PSI500 index (Figure 2). The ensemble mean values derived from the USFC index are 0.23 (−0.31)°(35 years)$^{-1}$ in the Northern (Southern) Hemisphere. All observed expansion rates in the Northern Hemisphere fall within the 5th–95th percentile span of MPI-GE (Figures 2a and 2c), indicating that the observed poleward expansion of the tropical belt from 1980 to 2014 is contained by the span of internal variability in the Northern Hemisphere. In the Southern Hemisphere, the observed tropical expansion rate derived from the ERAIM data set exceeded the MPI-GE range indicated by the PSI500 metric (Figure 2b).

3.2. IPO as the Dominant Internal Variability Mode

Earlier studies have indicated that a large part of the recent widening of the tropics is related to SST variability (Allen & Kovilakam, 2017), but there is a need to quantify the role of SST variations in explaining model–observation and intermodel differences. To answer the above questions, we examined the SST trends over the same period to identify the dominant internal SST mode. The observed poleward movement of the tropics coincides with notable SST cooling in the central-eastern tropical Pacific region and SST warming in the northwestern and southwestern subtropical Pacific regions (Figure 3a), resembling the SST patterns linked to the IPO (Henley et al., 2015). Hence, the expansion of the tropical belt in recent decades is likely influenced by SST

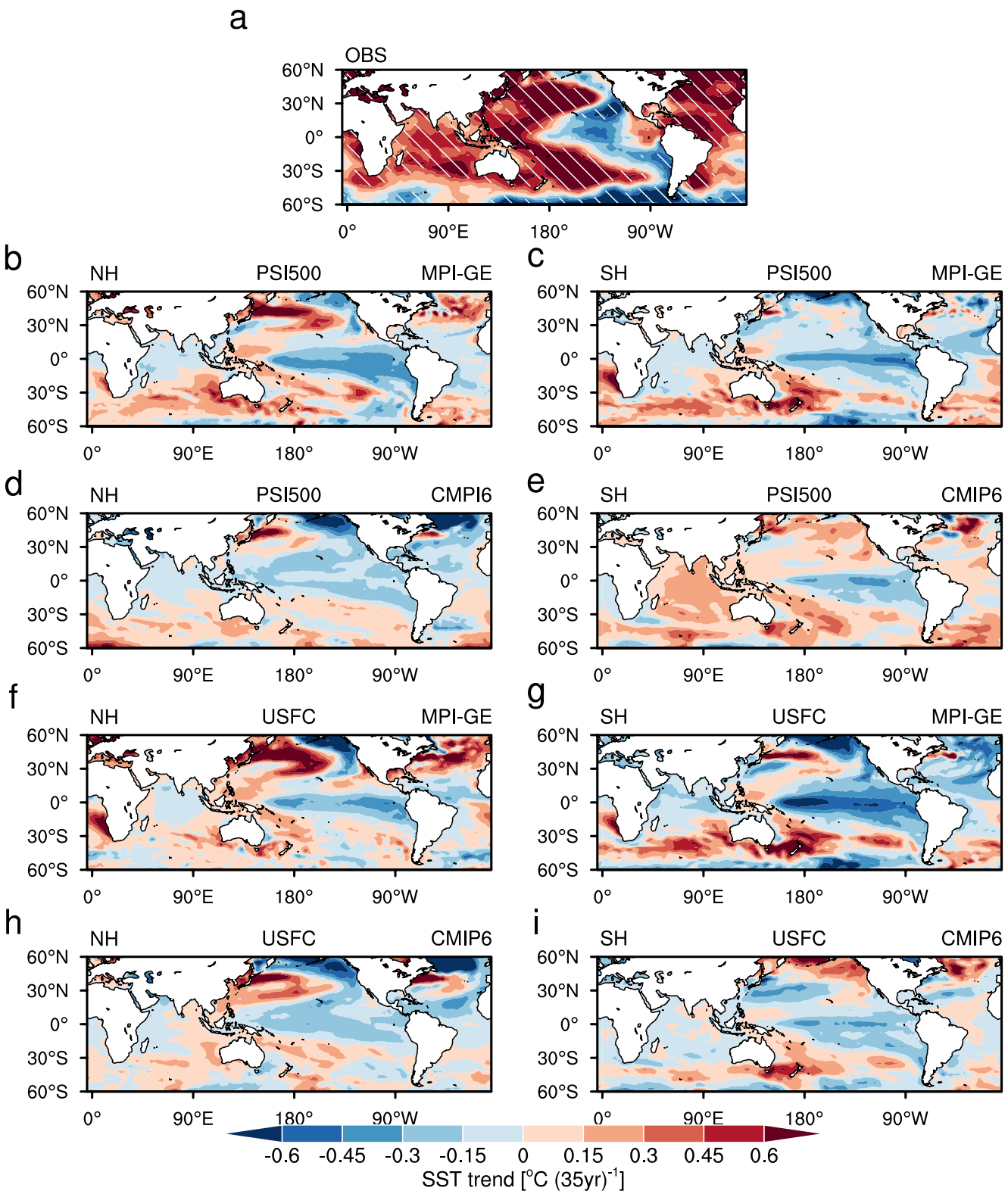

Figure 3. Spatial distributions of the SST trends from 1980 to 2014. (a) Observations. (b) Max10-Min10 composite differences of MPI-GE selected based on the PSI500 metric over the Northern Hemisphere and (c) Southern Hemisphere. Max10 (Min10) denotes the 10 ensemble members showing the maximum (minimum) tropical expansion rate in MPI-GE. (d, e) As in (b, c) but for the USFC metric. (f–i) As in (b–e) but for the CMIP6 models. Units: °C (35 years)$^{-1}$. The white slant hatchings denote where the trends are significant at the 95% confidence level.

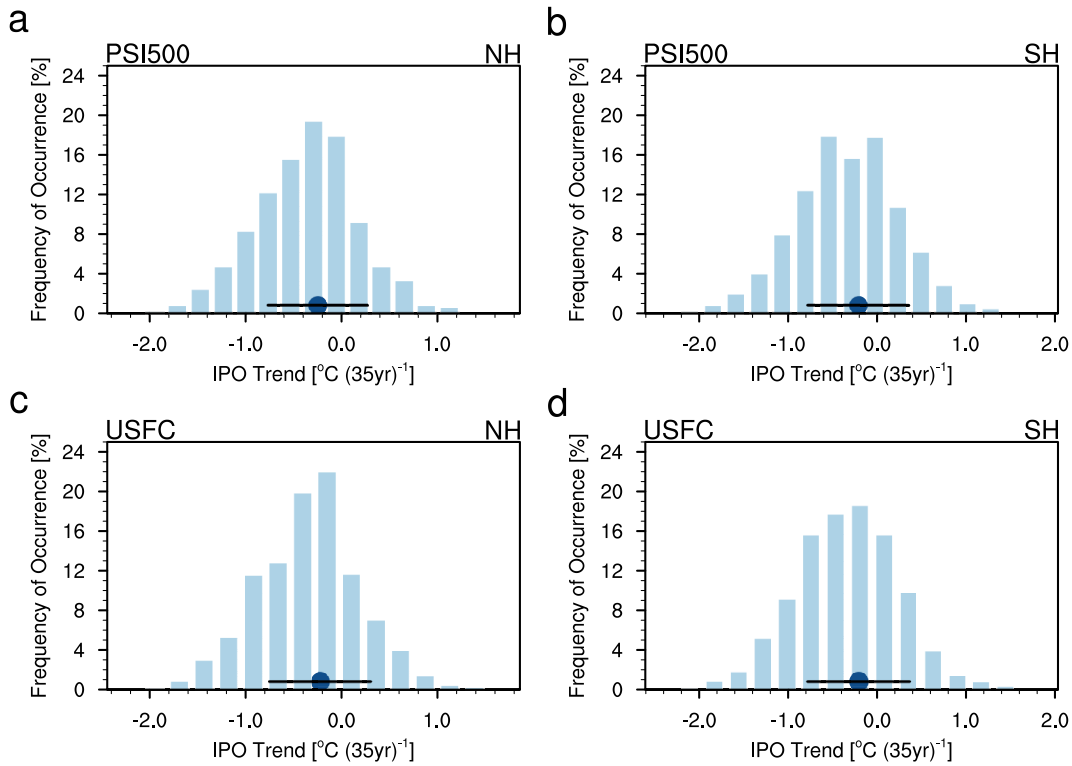

Figure 4. Confirming the role of the IPO. The distribution of the differences in IPO trends between the members with higher expansion rates and members with lower tropical expansion rates based on the PSI500 metric over the (a) Northern Hemisphere and (b) Southern Hemisphere. The blue dots and horizontal black lines denote the ensemble mean and one standard deviation range, respectively. (c, d) As in (a, b) but for the USFC metric.

anomalies associated with the negative phase of the IPO. To further test this hypothesis, we next extended our analysis to MPI-GE and examined whether the IPO phase could explain the spread among ensemble members. In MPI-GE, the difference in SST trends between the 10 members with the highest tropical expansion rate (Max10) and the 10 members with the lowest rate (Min10) exhibited patterns similar to those in the observations, displaying an IPO-like distribution (Figures 3b, 3c, 3f, and 3g). Similarly, the difference in SST trends in the CMIP6 models also resembled an IPO-like pattern (Figures 3d, 3e, 3h, and 3i). This indicates that the IPO plays a primary role in regulating the tropical belt width.

To confirm the above results, we examined the distribution of the differences in IPO trends between the different members of MPI-GE (Figure 4). We first randomly selected two members and compared their expansion rates to determine the higher and lower expansion rates. We then determined the difference in IPO trends between these two members by subtracting the IPO trends of the members with higher expansion rates from those with lower expansion rates. By repeating this process 1000 times, we could obtain the probability distribution of the differences in IPO trends corresponding to members with higher tropical expansion rates. We found that members showing a larger widening extent of the tropical width corresponded to more negative trends in the IPO in both hemispheres (Figure 4). This suggests that there is an association between tropical expansion and phase transition of the IPO. From 1980 to 2014, the IPO phase shifted from positive to negative, with SST cooling occurring over the eastern tropical Pacific (Dong & Dai, 2015).

The IPO-related SST change can influence the edges of the tropics by modulating the meridional temperature gradient (Yang et al., 2023). To explore how the phase shift of the IPO modulates the width of the tropical belt, we examined the differences in the composite air temperature between Max10 and Min10 (Figure 5). The composite result showed that accompanying the IPO phase transition, the tropical atmosphere cools, while the subtropical atmosphere warms. Consequently, the tropical-subtropical meridional temperature gradient is reduced; hence, the edge of the tropical belt shifts poleward (Lu et al., 2008). Note that despite a general decrease in the temperature gradient, the temperature changes in response to the IPO phase shift are asymmetric between the different

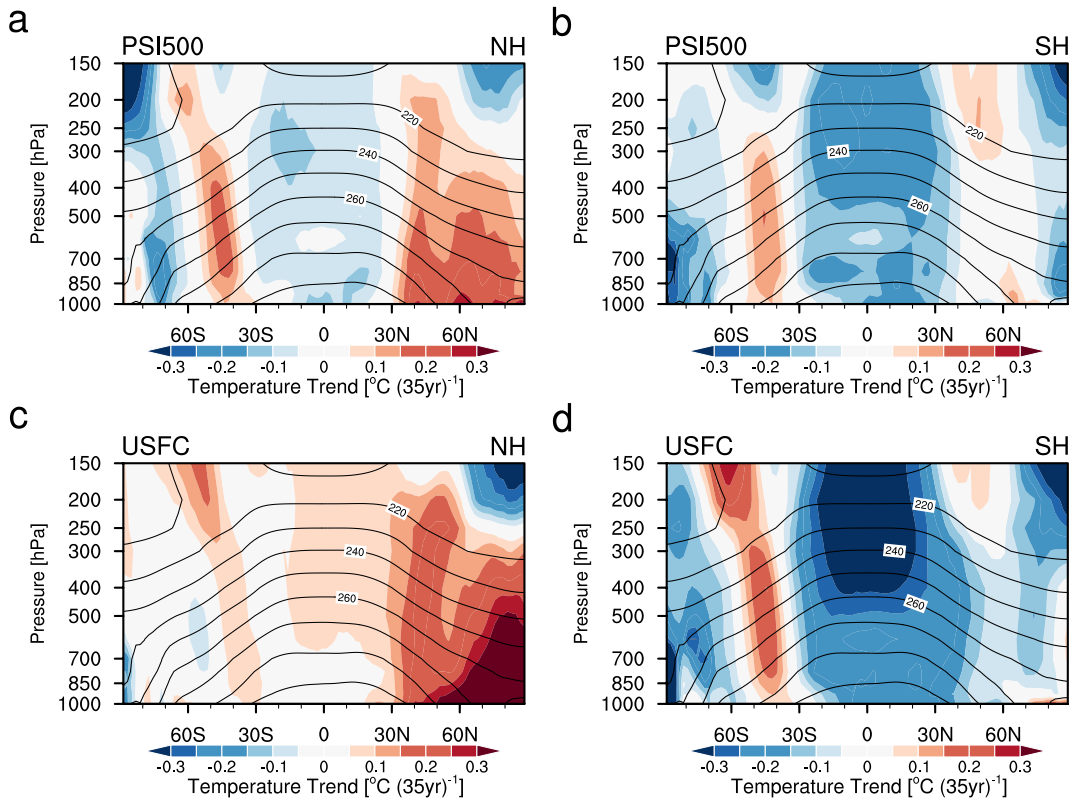

Figure 5. Mechanism of the influence of the IPO on the tropical belt width. (a) Max10-Min10 composite differences in the spatial distribution of the zonal-averaged air temperature trend (units: °C (35 years)$^{-1}$) over the Northern Hemisphere and (b) Southern Hemisphere based on the PSI500 metric. The black contours denote the climatological zonal-averaged air temperature. (c, d) As in (a, b) but for the USFC metric.

hemispheres. The positive-to-negative phase shift in the IPO primarily occurs at midlatitudes, as evidenced by the Max10-Min10 composites in the Northern Hemisphere. Conversely, in the Southern Hemisphere, these composites suggest a tendency toward cooling of the tropical atmosphere.

To further elucidate the role of the IPO, we examined the intermember relationship between the IPO phase change and the tropical expansion rate (Figure 6). We found that the tropical expansion rate is linearly correlated with the IPO phase change in both hemispheres, with a correlation coefficient of −0.55 (0.42) in the Northern (Southern) Hemisphere for the PSI500 metric (Figures 6a and 6b). We obtained similar results by using the USFC metric, with correlation coefficients of −0.53 in the Northern Hemisphere and 0.45 in the Southern Hemisphere (Figures 6c and 6d). This suggests that the positive-to-negative IPO phase transition induces a poleward shift in the tropical edge, and vice versa.

3.3. Quantifying the Contribution of the IPO to Tropical Expansion

Given the dominant internal variability mode of the IPO that modulates the extent of the tropical belt, we estimated the contribution of the IPO to the observed tropical expansion from 1980 to 2014 by adjusting the IPO phase transition in MPI-GE. The results showed that after adjustment, the IPO phase transition plays a major role in recent tropical expansion in the Northern Hemisphere, while the contribution of the IPO is comparable to that of external forcings in the Southern Hemisphere (Figure 7). This indicates that the influence of the IPO phase change superimposed on the external forcings led to widening of the tropical belt from 1980 to 2014. In the Northern Hemisphere, the MPI-GE ensemble mean reasonably reproduces the observed maximum tropical expansion rate after adjustment. Given that there is large spread among different reanalysis data sets in depicting tropical expansion rates in the Northern Hemisphere, we estimate the minimum relative contribution of IPO phase transition by dividing the IPO-adjusted tropical expansion rates with the maximum observational value. Quantitatively, the phase transition of the IPO explains at least 73% (66%) of the observed expansion rate based on the

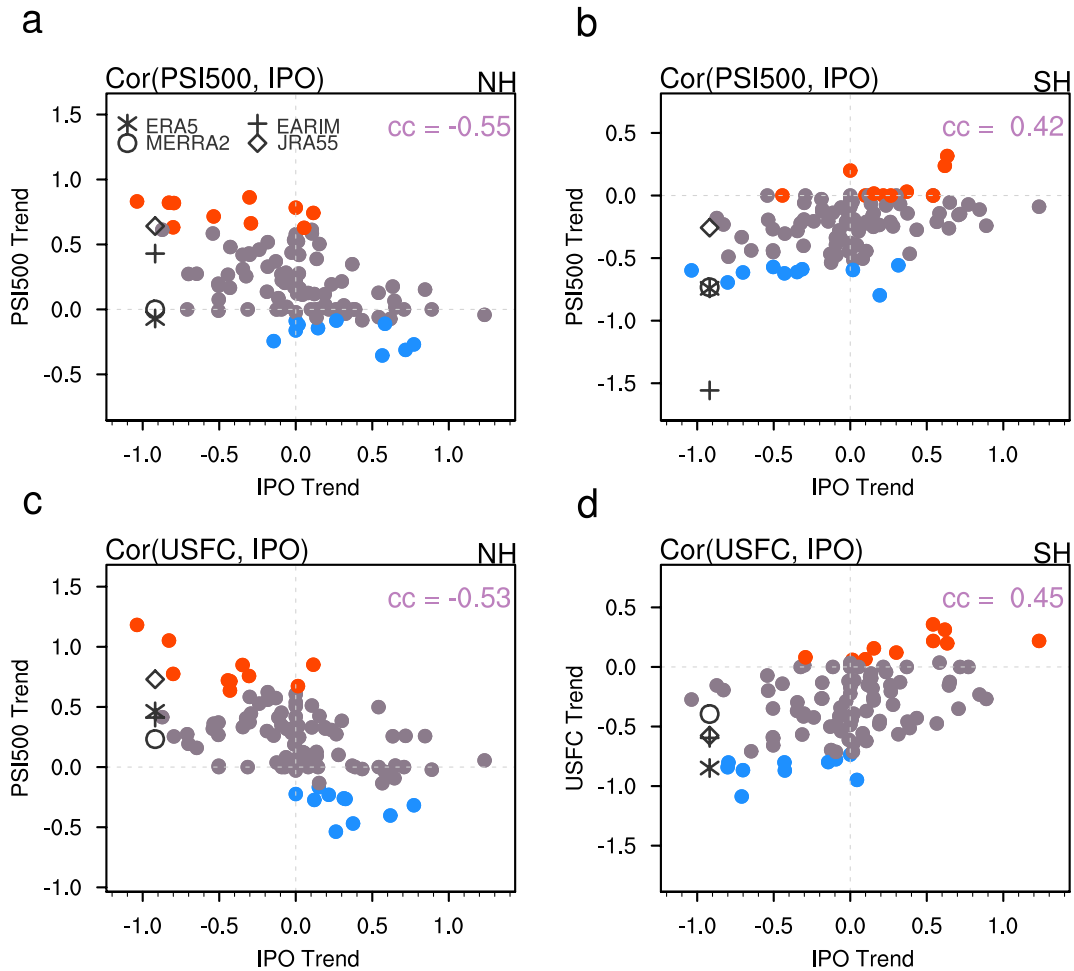

Figure 6. Relationships between the IPO trend (units: °C (35 years)$^{-1}$) and tropical expansion rate (units: degree (35 years)$^{-1}$) among the 100 MPI-GE members. Northern Hemisphere based on the (a) PSI500 metric and (c) USFC metric. The correlation coefficient (cc) is denoted in the upper right of the panel. The red (blue) dots denote the Max10 (Min10) members. The black diamonds, asterisks, circles and crosses denote the values from the different reanalysis data sets. (b, d) As in (a, c) but for the Southern Hemisphere.

PSI500 (USFC) metric (Figures 7a and 7c). Hence, the difference in tropical expansion observed in these models is due to the failure of the model to correctly reproduce the IPO phase transition. In addition, in the Southern Hemisphere, the IPO contributes only 27% to the observed trends for the PSI500 metric, while it explains approximately 64% of the observations for the USFC metric (Figures 7b and 7d). This uncertainty may be due to the higher sensitivity of the USFC metric to IPO phase changes. Hence, the internal variability can explain most of model–observation differences in the Northern Hemisphere, whereas it explains part of the differences in the Southern Hemisphere.

3.4. Impact of the IPO on Tropical Expansion-Related Precipitation Trends

The widening of the tropical belt has notably impacted hydroclimate changes, with critical societal and economic ramifications. To investigate the effect of tropical expansion on precipitation change, we show the spatial distributions of the tropical expansion-related precipitation trend during the 1980–2014 period in the observations and MPI-GE according to the PSI500 metric (Figures 8 and 9, respectively). Since the tropical belt contracts during El Niño events and expands during La Niña events on an interannual timescale (Lu et al., 2008), we also examine the effect of the ENSO on the tropical expansion-related precipitation trend (Section 2.6). We find that the extratropical precipitation response to tropical expansion remains unchanged in both hemispheres after subtracting the ENSO-congruent component of precipitation from each grid (Figures 8a–8d and 9a–9d).

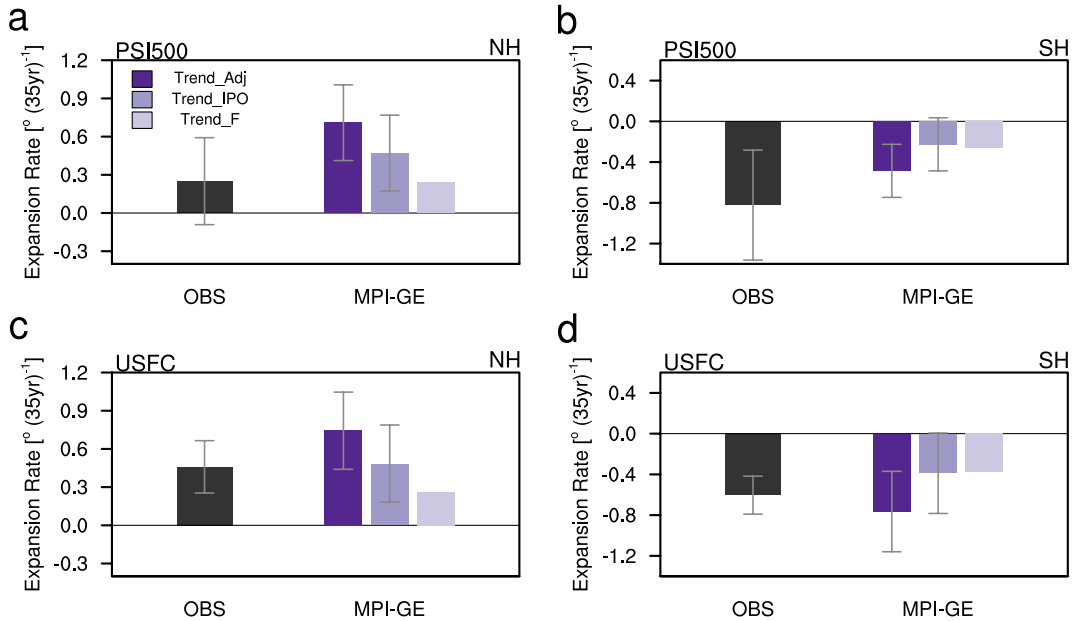

Figure 7. Quantifying the contribution of the IPO. (a) Adjustments in the tropical expansion rate based on the observed IPO phase transition over the Northern Hemisphere and (b) Southern Hemisphere based on the PSI500 metric. The black bar denotes the average tropical expansion rate derived from the different reanalysis data. The deep purple, purple and light purple bars denote the total expansion rate after adjustment (Trend_Adj), the IPO-related expansion rate (Trend_IPO), and the forced expansion rate (Trend_F) from the MPI-GE model, respectively. (c, d) As in (a, b) but for the USFC metric.

According to observations, the poleward movement of the tropical belt in the Northern Hemisphere is associated with the drying trend over subtropical regions, with decreases centered over the ocean (Figures 8a–8d). In the Southern Hemisphere, the poleward movement of the tropical belt drives a latitudinal zonal distribution of precipitation changes, with a drying trend between 30°S and 60°S and increased precipitation near 60°S (Figures 9a–9d).

Compared with the observations, the MPI-GE ensemble mean, which represents the impact of external forcings, can reproduce the related precipitation changes but with a far smaller magnitude than the observations (Figures 8c, 8d, 9c, and 9d). This indicates that external forcings alone cannot fully explain the observed tropical expansion-related precipitation trend. We then examine whether the IPO phase transition can explain the observation-model differences in tropical expansion-related precipitation changes (Figures 8e, 8f, 9e, and 9f). The results show that after adjusting the IPO phase transition in the MPI-GE members to be consistent with the observations, the MPI-GE ensemble mean exhibits similar characteristics to the observations with comparable magnitudes in both hemispheres (Figures 8e, 8f, 9e, and 9f). This suggests that the IPO is crucial for inducing the observed tropical expansion-related precipitation trend. Hence, both the IPO and external forcings contributed to the observed tropical expansion-related precipitation trend during the 1980–2014 period.

4. Discussion

This study relies on MPI-GE simulations. We also compared the results obtained from MPI-GE with those obtained from CESM-LE to verify the reliability of our conclusions. The tropical expansion rate is linearly correlated with IPO phase transition from 1980 to 2014 in both hemispheres in CESM-LE. The correlation coefficient is −0.50 (0.37) in the Northern (Southern) Hemisphere for the PSI500 metric (Figures 10a and 10b). Quantitatively, the IPO phase transition can explain at least 64% (35%) of the observed expansion rate in the Northern (Southern) Hemisphere based on the PSI500 metric in CESM-LE, comparable with that in MPI-GE (Figures 10c and 10d). The above analysis derived from CESM-LE further confirms the dominant role of the IPO in regulating the recent tropical expansion rate.

The main focus of this study is to explore how the IPO affects the tropical expansion rate. Notably, during the same period, the Atlantic Multidecadal Oscillation (AMO) (Schlesinger & Ramankutty, 1994), which is the

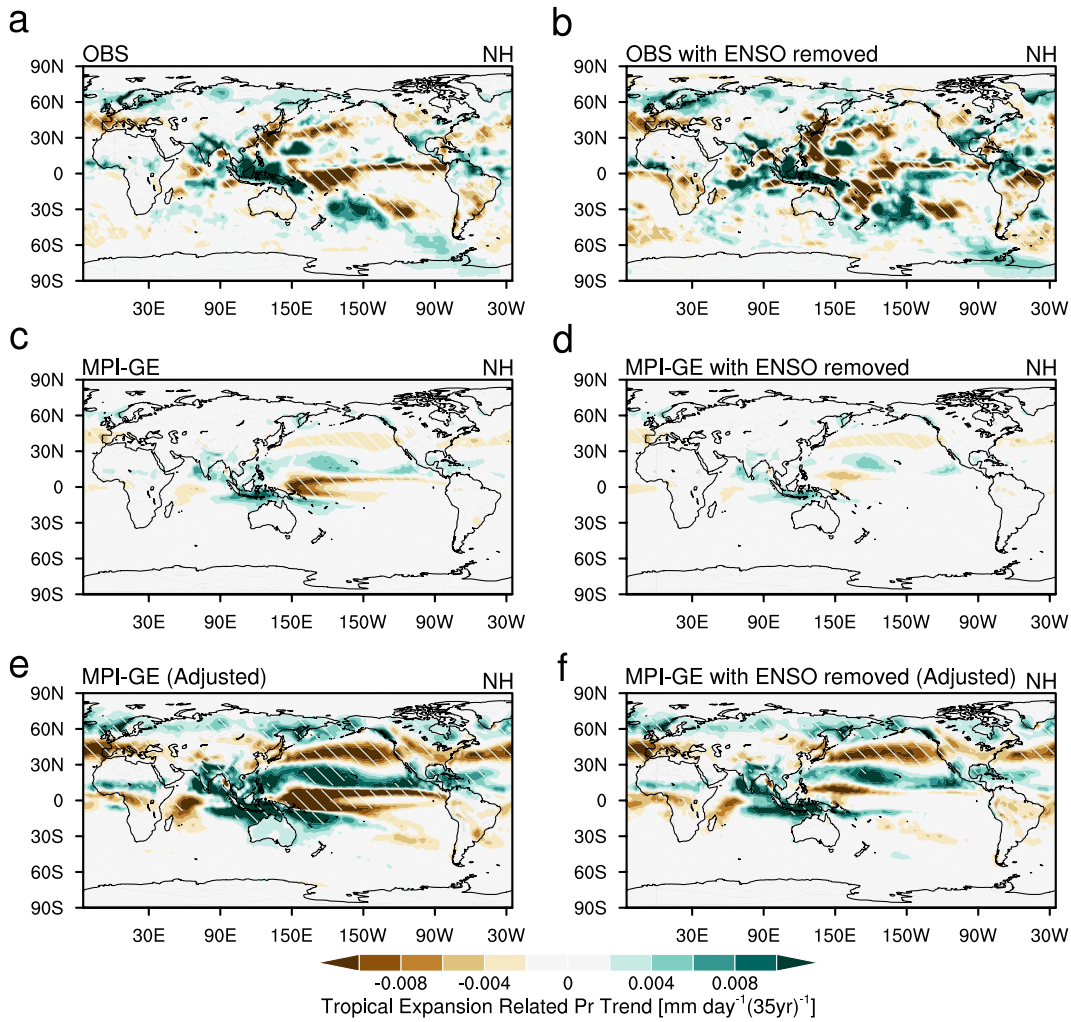

Figure 8. Impact of recent tropical expansion on precipitation changes. Changes in precipitation (units: mm day^{-1} (35 years)$^{-1}$) associated with tropical expansion based on the PSI500 metric in the Northern Hemisphere during 1980–2014 in (a) the observations; (c) MPI-GE ensemble mean; and (e) MPI-GE ensemble mean after adjustment of the tropical expansion rate based on the observed IPO phase transition. (b, d, f) As in (a, c, e) but influence of ENSO is removed. White slant hatchings in (a–f) denote areas where all (more than 80%) of the reanalysis (ensemble members) agree in sign.

leading mode of decadal variability in the North Atlantic Ocean, transitioned from a cold phase to a warm phase (Alexander et al., 2014). This shift in the AMO may also influence the extent of the tropical belt. To assess whether the phase shift of the AMO influenced the recent tropical expansion rate, we analyzed the correlation between the tropical expansion rate and AMO trend from 1980 to 2014 (Figure 11). Compared to that with the IPO trends, the correlation between the tropical expansion rate and AMO trends among the ensemble members is 0.16 (0.18) in the Northern (Southern) Hemisphere, indicating a nonsignificant role of the AMO. Additionally, internal atmospheric variability may contribute to tropical widening (Garfinkel et al., 2015; Grise et al., 2019; Simpson, 2018). However, further investigations are needed to determine the contribution of this internal atmospheric variability to recent tropical expansion.

The observed tropical expansion-related precipitation change shown here is like that of Schmidt and Grise (2017), who have found that the tropical expansion-related drying trend is stronger over oceans than over land. Schmidt and Grise (2017) proposed that tropical expansion is not associated with subtropical drying over land based on CMIP5 models. However, here we find that after the adjustment the widespread drought over the Northern Hemispheric continents, such as North America, Northeast Asia, and the Mediterranean region, can occur along with the northward shift of the Northern tropical edge (Figures 8c–8f). We have also examined the

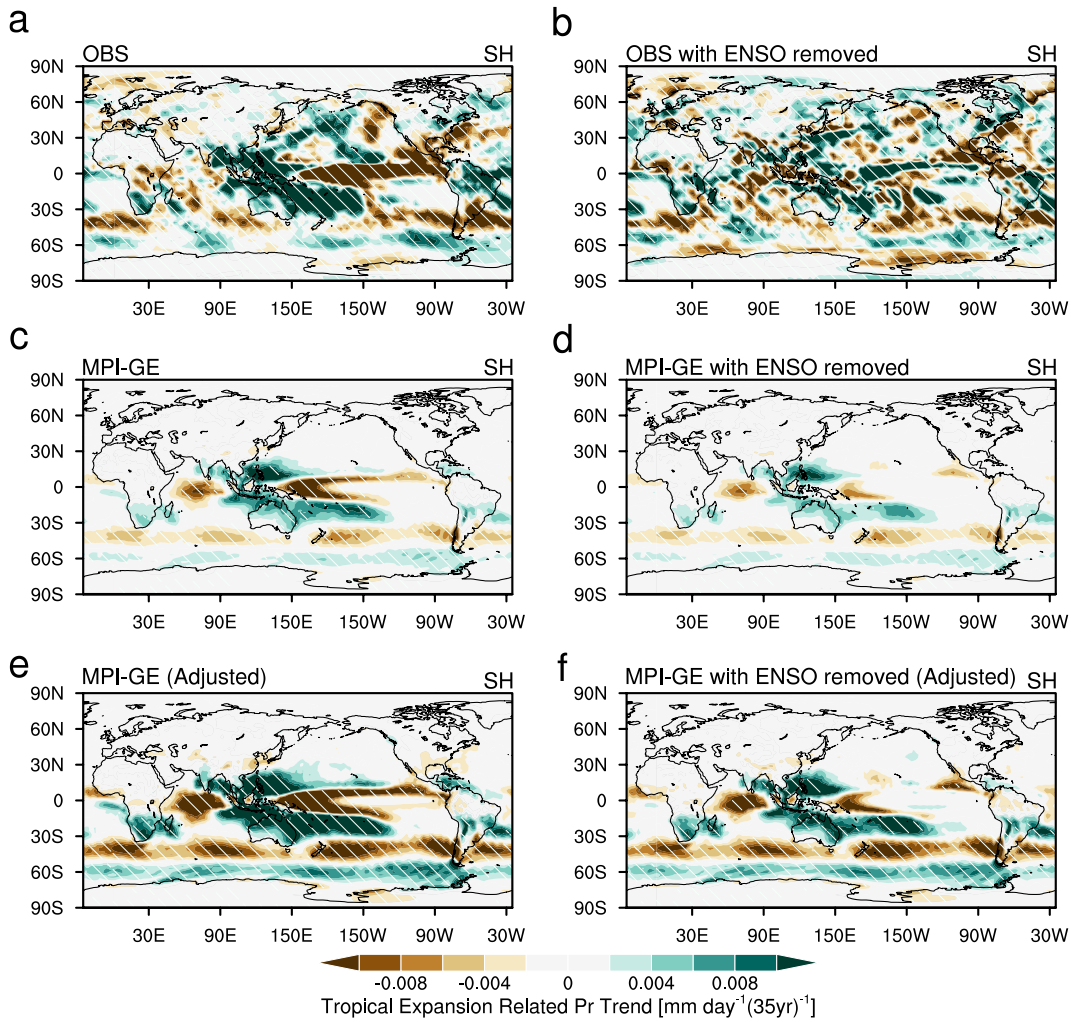

Figure 9. As in Figure 8 but for the Southern Hemisphere.

impact of IPO phase transition in tropical expansion-related precipitation changes in the Northern Hemisphere in CMIP6 models (Figure 12). The results further confirm that after adjusting the IPO phase transition in CMIP6 individual models with the observations, the CMIP6 ensemble mean also exhibits similar characteristics to the observations over land (Figures 8, 9, and 12). Therefore, we demonstrate that models' inability in reproducing the tropical expansion related-precipitation changes can be ascribed to the influence of internal IPO variability.

Another notable issue is the interhemispheric difference in the tropical expansion rate (Figures 1 and 2), which indicates a larger difference in the Southern Hemisphere than in the Northern Hemisphere. This difference in the tropical expansion rate between hemispheres can be attributed to the influence of ozone holes (Grise & Davis, 2020; Grise et al., 2019; D. W. J. Thompson & Solomon, 2002). In the Southern Hemisphere, the poleward expansion of the tropical belt is partially driven by stratospheric ozone depletion. Conversely, the Northern Hemisphere has experienced relatively limited ozone loss. Furthermore, greenhouse gas forcing can result in interhemispheric differences in the tropical expansion rate, leading to interhemispheric variations in static stability across subtropical regions (Watt-Meyer et al., 2019). Specifically, the Northern Hemisphere will undergo smaller changes in static stability under the influence of greenhouse gas warming than the Southern Hemisphere, which will exhibit a lower sensitivity to such changes (Watt-Meyer et al., 2019).

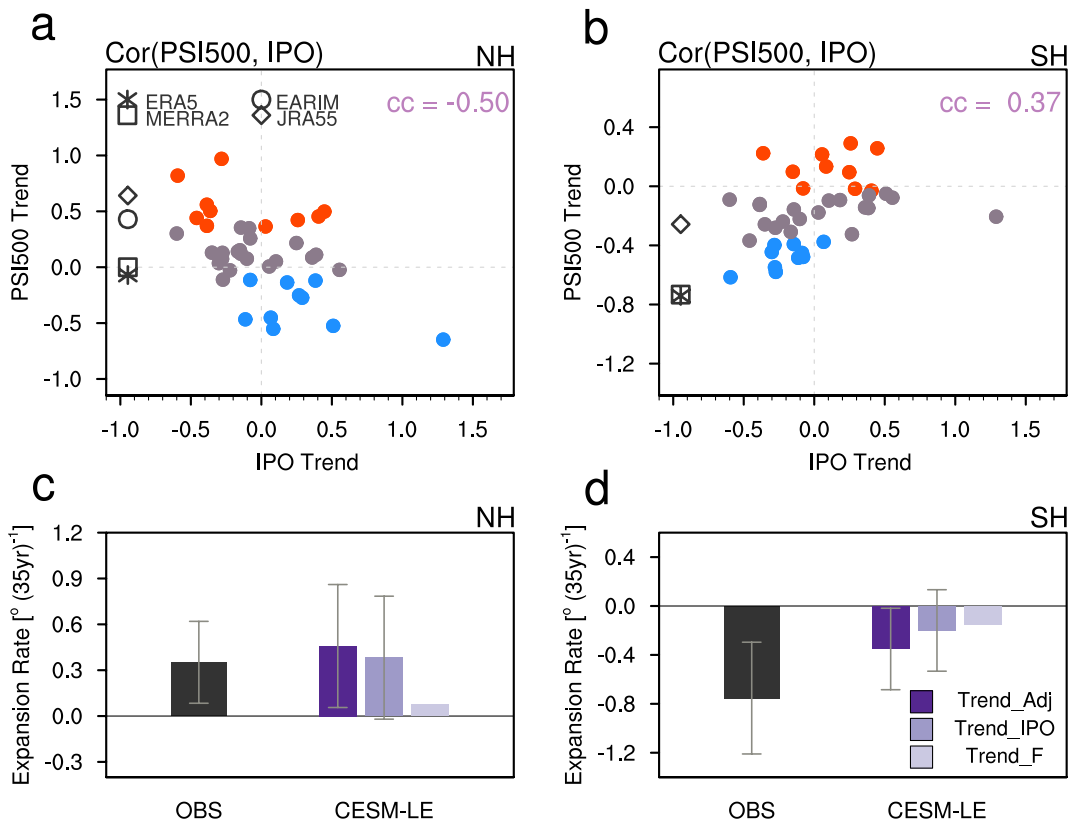

Figure 10. Role of the IPO in recent tropical expansion in CESM-LE. (a, b) As in Figures 6a and 6b but for CESM-LE. (c, d) As in Figures 7a and 7b but for CESM-LE.

5. Concluding Remarks

The mechanism underlying the model–observation differences and the intermodel spread in recent tropical expansion rates has been a subject of great concern, but whether internal variability can quantitatively explain these differences and spread has not been determined. Here, by combining multiple lines of evidence from both reanalysis data and initial-condition large-ensemble simulations and complemented with CMIP6 simulations, we demonstrate that tropical expansion over the 1980–2014 period is largely attributed to internal variability linked to the IPO. The IPO phase transition from positive to negative during this period reduced the equator-to-pole

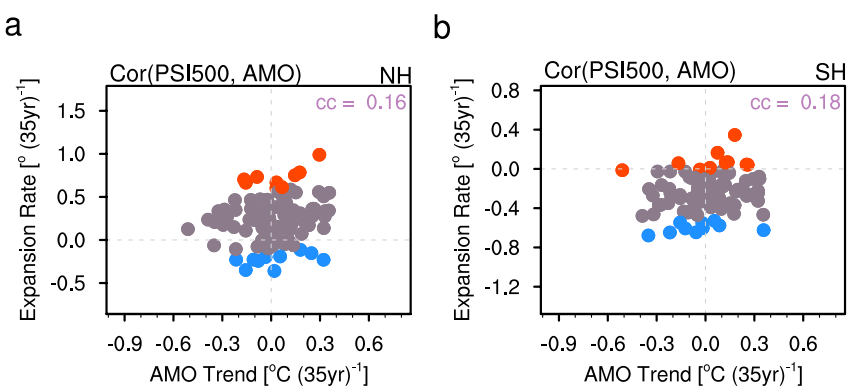

Figure 11. Relationships between the AMO trend (units: °C (35 years)$^{-1}$) and tropical expansion rate (units: degree (35 years)$^{-1}$) among the 100 MPI-GE members based on the PSI500 metric. (a) Northern Hemisphere and (b) Southern Hemisphere. The correlation coefficient (cc) is denoted in the upper right of the panel. The red (blue) dots denote the Max10 (Min10) members.

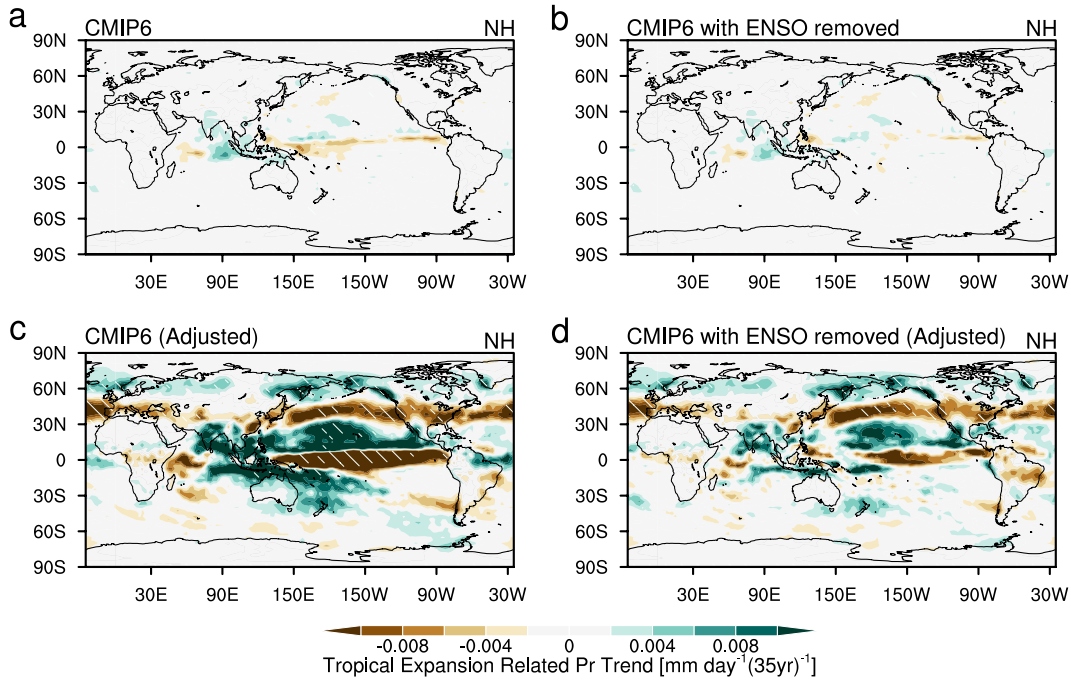

Figure 12. As in Figures 8c–8f but for CMIP6 models. White slant hatchings denote areas where more than 80% of the models agree in sign.

temperature gradient and hence forced the subtropical edges of the tropics to move toward higher latitudes in both hemispheres. After using the observed IPO trend to adjust the model-simulated IPO trends, we found that the phase shift of the IPO could explain at least 73% (66%) of the observed tropical expansion rate based on the PSI500 (USFC) metric in the Northern Hemisphere. In the Southern Hemisphere, the IPO could contribute approximately 27% to the observed tropical expansion rate for the PSI500 metric and 64% for the USFC metric. IPO also plays a crucial role in shaping changes in precipitation associated with tropical expansion. Given the substantial influence of the internal variability of the IPO, our results highlight the importance of using models with large ensemble members to accurately assess the ability of these models to reproduce the observed tropical expansion rate. Our findings could help to reconcile the longstanding model–observation inconsistency.

Data Availability Statement

All data used in this study are available to the public. The ERAIM reanalysis data are available at Dee et al. (2011). The ERA5 reanalysis data can be found at Hersbach et al. (2017). The MERRA2 reanalysis data can be obtained at Global Modeling and Assimilation Office (GMAO) (2015). The JRA55 reanalysis data sets (Kobayashi et al., 2015) are provided from the Japanese 55-year Reanalysis (JRA-55) project carried out by the Japan Meteorological Agency (JMA). The monthly mean SST from the ERSSTv5 data set can be downloaded at B. Huang et al. (2017). The GPCP data are publicly available from Adler et al. (2018). The MPI-GE data can be obtained at Maher et al. (2019). The CESM-LE data are available at Kay et al. (2015). The CMIP6 data can be found in the Eyring et al. (2016).

Acknowledgments
This study was supported by the National Natural Science Foundation of China under Grant 41988101. M.W. was supported by the China Postdoctoral Science Foundation (2023M733292), the Open Project (Project No. KLME202302) of the Key Laboratory of Meteorological Disaster (KLME), the Ministry of Education & Collaborative Innovation Center on Forecast and Evaluation of Meteorological Disasters (CIC-FEMD), and the "CUG Scholar" Scientific Research Funds at China University of Geosciences (Wuhan) (Project No. 2022120). C.L. was supported by the Clusters of Excellence CLICCS (EXC2037), University of Hamburg, funded by the German Research Foundation (DFG). We also acknowledge the support provided by the Jiangsu Collaborative Innovation Center for Climate Change.

References

Adam, O., Grise, K. M., Staten, P., Simpson, I. R., Davis, S. M., Davis, N. A., et al. (2018). The TropD software package (v1): Standardized methods for calculating tropical-width diagnostics. *Geoscientific Model Development*, *11*(10), 4339–4357. https://doi.org/10.5194/gmd-11-4339-2018

Adler, R. F., Huffman, G. J., Chang, A., Ferraro, R., Xie, P., Janowiak, J., et al. (2003). The version 2 Global Precipitation Climatology Project (GPCP) monthly precipitation analysis (1979-present). *Journal of Hydrometeorology*, *4*(6), 1147–1167. https://doi.org/10.1175/1525-7541(2003)004<1147:TVGPCP>2.0.CO;2

Adler, R. F., Sapiano, M. R. P., Huffman, G. J., Wang, J.-J., Gu, G., Bolvin, D., et al. (2018). The Global Precipitation Climatology Project (GPCP) monthly analysis (new version 2.3) and a review of 2017 global precipitation [Dataset]. *Atmosphere*, *9*(4), 138. https://doi.org/10.3390/atmos9040138

Alexander, M. A., Halimeda Kilbourne, K., & Nye, J. A. (2014). Climate variability during warm and cold phases of the Atlantic Multidecadal Oscillation (AMO) 1871–2008. *Journal of Marine Systems*, *133*, 14–26. https://doi.org/10.1016/j.jmarsys.2013.07.017

Allen, R. J., & Kovilakam, M. (2017). The role of natural climate variability in recent tropical expansion. *Journal of Climate*, *30*(16), 6329–6350. https://doi.org/10.1175/JCLI-D-16-0735.1

Allen, R. J., Sherwood, S. C., Norris, J. R., & Zender, C. S. (2012). Recent Northern Hemisphere tropical expansion primarily driven by black carbon and tropospheric ozone. *Nature*, *485*(7398), 350–354. https://doi.org/10.1038/nature11097

Brönnimann, S., Fischer, A. M., Rozanov, E., Poli, P., Compo, G. P., & Sardeshmukh, P. D. (2015). Southward shift of the northern tropical belt from 1945 to 1980. *Nature Geoscience*, *8*(12), 969–974. https://doi.org/10.1038/NGEO2568

Chen, G., Lu, J., & Frierson, D. M. W. (2008). Phase speed spectra and the latitude of surface westerlies: Interannual variability and global warming trend. *Journal of Climate*, *21*(22), 5942–5959. https://doi.org/10.1175/2008JCLI2306.1

Cook, K. H. (2003). Role of continents in driving the Hadley cells. *Journal of the Atmospheric Sciences*, *60*(7), 957–976. https://doi.org/10.1175/1520-0469(2003)060<0957:Rocidt>2.0.Co;2

Davis, N. A., & Birner, T. (2017). On the discrepancies in tropical belt expansion between reanalyses and climate models and among tropical belt width metrics. *Journal of Climate*, *30*(4), 1211–1231. https://doi.org/10.1175/JCLI-D-16-0371.1

Davis, N. A., & Davis, S. M. (2018). Reconciling Hadley cell expansion trend estimates in reanalyses. *Geophysical Research Letters*, *45*(20), 11439–11446. https://doi.org/10.1029/2018gl079593

Davis, S. M., & Rosenlof, K. H. (2012). A multidiagnostic intercomparison of tropical-width time series using reanalyses and satellite observations. *Journal of Climate*, *25*(4), 1061–1078. https://doi.org/10.1175/JCLI-D-11-00127.1

Dee, D. P., Uppala, S. M., Simmons, A. J., Berrisford, P., Poli, P., Kobayashi, S., et al. (2011). ERA-Interim global atmospheric reanalysis [Dataset]. *Copernicus Climate Change Service (C3S) Climate Data Store (CDS)*. https://doi.org/10.24381/cds.f2f5241d

Deser, C., Lehner, F., Rodgers, K. B., Ault, T., Delworth, T. L., DiNezio, P. N., et al. (2020). Insights from Earth system model initial-condition large ensembles and future prospects. *Nature Climate Change*, *10*(4), 277–286. https://doi.org/10.1038/s41558-020-0731-2

Dong, B., & Dai, A. (2015). The influence of the Interdecadal Pacific Oscillation on temperature and precipitation over the Globe. *Climate Dynamics*, *45*(9–10), 2667–2681. https://doi.org/10.1007/s00382-015-2500-x

Eyring, V., Bony, S., Meehl, G. A., Senior, C. A., Stevens, B., Stouffer, R. J., & Taylor, K. E. (2016). Overview of the Coupled model Intercomparison Project Phase 6 (CMIP6) experimental design and organization [Dataset]. *Geoscientific Model Development*, *9*, 1937–1958. https://doi.org/10.5194/gmd-9-1937-2016

Feng, S., & Fu, Q. (2013). Expansion of global drylands under a warming climate. *Nature Climate Change*, *10*, 7–10. https://doi.org/10.5194/acpd-13-14637-2013

Fu, Q., Johanson, C. M., Wallace, J. M., & Reichler, T. (2006). Enhanced mid-latitude tropospheric warming in satellite measurements. *Science*, *312*(5777), 1179. https://doi.org/10.1126/science.1125566

Garfinkel, C. I., Waugh, D. W., & Polvani, L. M. (2015). Recent Hadley cell expansion: The role of internal atmospheric variability in reconciling modeled and observed trends. *Geophysical Research Letters*, *42*(24), 10824–10831. https://doi.org/10.1002/2015GL066942

Gelaro, R., McCarty, W., Suarez, M. J., Todling, R., Molod, A., Takacs, L., et al. (2017). The Modern-Era Retrospective Analysis for Research and Applications, Version 2 (MERRA-2) [Dataset]. *Journal of Climate*, *30*, 5419–5454. https://doi.org/10.1175/jcli-d-16-0758.1

Grise, K. M., & Davis, S. M. (2020). Hadley cell expansion in CMIP6 models. *Atmospheric Chemistry and Physics*, *20*(9), 5249–5268. https://doi.org/10.5194/acp-20-5249-2020

Grise, K. M., Davis, S. M., Simpson, I. R., Waugh, D. W., Fu, Q., Allen, R. J., et al. (2019). Recent tropical expansion: Natural variability or forced response? *Journal of Climate*, *32*(5), 1551–1571. https://doi.org/10.1175/JCLI-D-18-0444.1

Grise, K. M., Davis, S. M., Staten, P. W., & Adam, O. (2018). Regional and seasonal characteristics of the recent expansion of the tropics. *Journal of Climate*, *31*(17), 6839–6856. https://doi.org/10.1175/JCLI-D-18-0060.1

Henley, B. J., Gergis, J., Karoly, D. J., Power, S., Kennedy, J., & Folland, C. K. (2015). A tripole index for the interdecadal Pacific Oscillation. *Climate Dynamics*, *45*(11–12), 3077–3090. https://doi.org/10.1007/s00382-015-2525-1

Hersbach, H., Bell, B., Berrisford, P., Hirahara, S., Horányi, A., Muñoz-Sabater, J., et al. (2017). Complete ERA5 from 1940: Fifth generation of ECMWF atmospheric reanalyses of the global climate [Dataset]. *Copernicus Climate Change Service (C3S) Data Store (CDS)*. https://doi.org/10.24381/cds.143582cf

Hersbach, H., Bell, B., Berrisford, P., Hirahara, S., Horányi, A., Muñoz-Sabater, J., et al. (2020). The ERA5 global reanalysis. *Quarterly Journal of the Royal Meteorological Society*, *146*(730), 1999–2049. https://doi.org/10.1002/qj.3803

Hu, Y., & Fu, Q. (2007). Observed poleward expansion of the Hadley circulation since 1979. *Atmospheric Chemistry and Physics*, *7*(19), 5229–5236. https://doi.org/10.5194/acp-7-5229-2007

Hu, Y., Tao, L., & Liu, J. (2013). Poleward expansion of the Hadley circulation in CMIP5 simulations. *Advances in Atmospheric Sciences*, *30*(3), 790–795. https://doi.org/10.1007/s00376-012-2187-4

Huang, B., Thorne, P. W., Banzon, V. F., Boyer, T., Chepurin, G., Lawrimore, J. H., et al. (2017). NOAA Extended Reconstructed Sea Surface Temperature (ERSST), version 5. [ERSST v5] [Dataset]. *NOAA National Centers for Environmental Information*. [31-01-2024]. https://doi.org/10.7289/V5T72FNM

Huang, X., Zhou, T., Turner, A., Dai, A., Chen, X., Clark, R., et al. (2020). The recent decline and recovery of Indian Summer Monsoon Rainfall: Relative roles of external forcing and internal variability. *Journal of Climate*, *33*(12), 5035–5060. https://doi.org/10.1175/JCLI-D-19-0833.1

Hudson, R. D., Andrade, M. F., Follette, M. B., & Frolov, A. D. (2006). The total ozone field separated into meteorological regimes—Part II: Northern Hemisphere mid-latitude total ozone trends. *Atmospheric Chemistry and Physics*, *6*(12), 5183–5191. https://doi.org/10.5194/acp-6-5183-2006

Irwin, A. J., & Oliver, M. J. (2009). Are ocean deserts getting larger? *Geophysical Research Letters*, *36*(18), L18609. https://doi.org/10.1029/2009GL039883

Johanson, C. M., & Fu, Q. (2009). Hadley cell widening: Model simulations versus observations. *Journal of Climate*, *22*(10), 2713–2725. https://doi.org/10.1175/2008JCLI2620.1

Kay, J. E., Deser, C., Phillips, A., Mai, A., Hannay, C., Strand, G., et al. (2015). The Community Earth System Model (CESM) large ensemble project: A community resource for studying climate change in the presence of internal climate variability [Dataset]. *Bulletin of the American Meteorological Society*, *96*, 1333–1349. https://doi.org/10.1175/BAMS-D-13-00255.1

Kobayashi, S., Ota, Y., Harada, Y., Ebita, A., Moriya, M., Onoda, H., et al. (2015). The JRA-55 reanalysis: General specifications and basic characteristics [Dataset]. *Journal of the Meteorological Society of Japan. Series II*, *93*, 5–48. https://doi.org/10.2151/jmsj.2015-001

Lu, J., Chen, G., & Frierson, D. M. W. (2008). Response of the zonal mean atmospheric circulation to El Niño versus global warming. *Journal of Climate*, *21*(22), 5835–5851. https://doi.org/10.1175/2008JCLI2200.1

Maher, N., Milinski, S., Suarez-Gutierrez, L., Botzet, M., Dobrynin, M., Kornblueh, L., et al. (2019). The Max Planck Institute Grand ensemble: Enabling the exploration of climate system variability. [Dataset]. *Journal of Advances in Modeling Earth Systems*, *11*, 2050–2069. https://doi.org/10.1029/2019MS001639

Mantsis, D. F., Sherwood, S., Allen, R., & Shi, L. (2017). Natural variations of tropical width and recent trends. *Geophysical Research Letters*, *44*(8), 3825–3832. https://doi.org/10.1002/2016gl072097

Mantua, N. J., & Hare, S. R. (2002). The Pacific decadal oscillation. *Journal of Oceanography*, *58*(1), 35–44. https://doi.org/10.1023/A:1015820616384

Moore, J. K., Fu, W., Primeau, F., Britten, G. L., Lindsay, K., Long, M., et al. (2018). Sustained climate warming drives declining marine biological productivity. *Science*, *359*(6380), 1139–1143. https://doi.org/10.1126/science.aao6379

Nguyen, H., Evans, A., Lucas, C., Smith, I., & Timbal, B. (2013). The Hadley circulation in reanalyses: Climatology, variability, and change. *Journal of Climate*, *26*(10), 3357–3376. https://doi.org/10.1175/JCLI-D-12-00224.1

Notz, D. (2015). How well must climate models agree with observations? *Philosophical Transactions of the Royal Society A*, *373*(2052), 20140164. https://doi.org/10.1098/rsta.2014.0164

Polovina, J. J., Howell, E. A., & Abecassis, M. (2008). Ocean's least productive waters are expanding. *Geophysical Research Letters*, *35*(3), L03618. https://doi.org/10.1029/2007GL031745

Post, D. A., Timbal, B., Chiew, F. H. S., Hendon, H. H., Nguyen, H., & Moran, R. (2014). Decrease in southeastern Australian water availability linked to ongoing Hadley cell expansion. *Earth's Future*, *2*(4), 231–238. https://doi.org/10.1002/2013ef000194

Quan, X.-W., Hoerling, M. P., Perlwitz, J., Diaz, H. F., & Xu, T. (2014). How fast are the tropics expanding? *Journal of Climate*, *27*(5), 1999–2013. https://doi.org/10.1175/JCLI-D-13-00287.1

Rykaczewski, R. R., Dunne, J. P., Sydeman, W. J., García-Reyes, M., Black, B. A., & Bograd, S. J. (2015). Poleward displacement of coastal upwelling-favorable winds in the ocean's eastern boundary currents through the 21st century. *Geophysical Research Letters*, *42*(15), 6424–6431. https://doi.org/10.1002/2015gl064694

Salzmann, M., & Cherian, R. (2015). On the enhancement of the Indian summer monsoon drying by Pacific multidecadal variability during the latter half of the twentieth century. *Journal of Geophysical Research: Atmospheres*, *120*(18), 9103–9118. https://doi.org/10.1002/2015jd023313

Scheff, J., & Frierson, D. M. W. (2012). Robust future precipitation declines in CMIP5 largely reflect the poleward expansion of model subtropical dry zones. *Geophysical Research Letters*, *39*(18), L18704. https://doi.org/10.1029/2012GL052910

Schlesinger, M. E., & Ramankutty, N. (1994). An oscillation in the global cliamte system of period 65-70 years. *Nature*, *372*(6506), 508–509. https://doi.org/10.1038/372508a0

Schmidt, D. F., & Grise, K. M. (2017). The response of local precipitation and sea level pressure to Hadley cell expansion. *Geophysical Research Letters*, *44*(20), 10573–10582. https://doi.org/10.1002/2017gl075380

Seidel, D. J., Fu, Q., Randel, W. J., & Reichler, T. J. (2008). Widening of the tropical belt in a changing climate. *Nature Geoscience*, *1*, 21–24. https://doi.org/10.1038/ngeo.2007.38

Seidel, D. J., & Randel, W. J. (2007). Recent widening of the tropical belt: Evidence from tropopause observations. *Journal of Geophysical Research*, *112*(D20), D20113. https://doi.org/10.1029/2007JD008861

Seo, K.-H., Yoon, S.-P., Lu, J., Hu, Y., Staten, P. W., & Frierson, D. M. W. (2023). What controls the interannual variation of hadley cell extent in the Northern Hemisphere: Physical mechanism and empirical model for edge variation. *npj Climate and Atmospheric Science*, *6*(1), 204. https://doi.org/10.1038/s41612-023-00533-w

Sharmila, S., & Walsh, K. J. E. (2018). Recent poleward shift of tropical cyclone formation linked to Hadley cell expansion. *Nature Climate Change*, *8*(8), 730–736. https://doi.org/10.1038/s41558-018-0227-5

Simpson, I. R. (2018). Natural variability in the width of the tropics. In *US CLIVAR VARIATIONS* (Vol. 16, pp. 14–20). U.S. CLIVAR Project Office

Staten, P. W., Grise, K. M., Davis, S. M., Karnauskas, K. B., Waugh, D. W., Maycock, A. C., et al. (2020). Tropical widening: From global variations to regional impacts. *Bulletin of the American Meteorological Society*, *101*(6), E897–E904. https://doi.org/10.1175/BAMS-D-19-0047.1

Staten, P. W., Lu, J., Grise, K. M., Davis, S. M., & Birner, T. (2018). Re-examining tropical expansion. *Nature Climate Change*, *8*(9), 768–775. https://doi.org/10.1038/s41558-018-0246-2

Studholme, J., & Gulev, S. (2018). Concurrent changes to Hadley circulation and the meridional distribution of tropical cyclones. *Journal of Climate*, *31*(11), 4367–4389. https://doi.org/10.1175/JCLI-D-17-0852.1

Tao, L., Hu, Y., & Liu, J. (2015). Anthropogenic forcing on the Hadley circulation in CMIP5 simulations. *Climate Dynamics*, *46*(9–10), 3337–3350. https://doi.org/10.1007/s00382-015-2772-1

Thompson, D., Wallace, J., & Hegerl, G. (2000). Annular modes in the extratropical circulation. Part II: Trends. *Journal of Climate*, *13*(5), 1018–1036. https://doi.org/10.1175/1520-0442(2000)013<1018:AMITEC>2.0.CO;2

Thompson, D. W. J., & Solomon, S. (2002). Interpretation of recent Southern Hemisphere climate change. *Science*, *296*(5569), 895–899. https://doi.org/10.1126/science.1069270

Watt-Meyer, O., Frierson, D. M. W., & Fu, Q. (2019). Hemispheric asymmetry of tropical expansion under CO_2 forcing. *Geophysical Research Letters*, *46*(15), 9231–9240. https://doi.org/10.1029/2019gl083695

Wu, M., Zhou, T., Li, C., Li, H., Chen, X., Wu, B., et al. (2021). A very likely weakening of Pacific Walker Circulation in constrained near-future projections. *Nature Communications*, *12*(1), 6502. https://doi.org/10.1038/s41467-021-26693-y

Xian, T., Xia, J., Wei, W., Zhang, Z., Wang, R., Wang, L.-P., & Ma, Y.-F. (2021). Is Hadley cell expanding? *Atmosphere*, *12*(12), 1699. https://doi.org/10.3390/atmos12121699

Yang, H., Lohmann, G., Shi, X., & Müller, J. (2023). Evaluating the mechanism of tropical expansion using idealized numerical experiments. *Ocean-Land-Atmosphere Research*, *2*, 0004. https://doi.org/10.1029/2019gl083695

Yeh, S. W., Hyun, S. H., Park, I. H., & Zheng, X. T. (2021). Surface temperature variability in climate models with large and small internal climate variability. *Quarterly Journal of the Royal Meteorological Society*, *147*(738), 3004–3016. https://doi.org/10.1002/qj.4112

Zhou, T., & Li, J. (2008). Climate change in China congruent with the linear trends of the annular modes. *Atmospheric and Oceanic Science Letters*, *1*, 1–7. https://doi.org/10.1080/16742834.2008.11446760